ISSN: 2181-3337 | SCIENTISTS.UZ VOLUME 5 ISSUE 9 | SEPTEMBER 2026

ASSESSMENT OF RADIONUCLIDE PARAMETERS IN SOILS OF RECLAIMED AREAS BASED ON A MATHEMATICAL MODEL

Akbarova Nigora[1], Toshpulatova Dilorom[2,3]

Tashkent State Technical University (TSTU), Tashkent, Uzbekistan[1]
Joint Belorussian–Uzbek Intersectoral Institute of Applied Technical Qualifications in Tashkent, Uzbekistan[2]
Shahrisabz State Pedagogical Institute, Shahrisabz, Uzbekistan[3]

DOI: 10.67620/sai.59a0009

ABSTRACT

Digital holographic interferometry (DHI) requires phase maps to be denoised and unwrapped before reliable displacement can be recovered. Learning-based approaches increasingly address these tasks, but their development requires paired data with known ground-truth displacement, which experimental holograms rarely provide. This study develops a forward model of the DHI measurement chain and a synthetic phase-map generator, then uses them to identify the operating limits of a classical phase-processing pipeline. The model relates interferometric phase to displacement, incorporates multiplicative speckle decorrelation dependent on local fringe density, and adds detector noise. Ground-truth displacement fields are derived from analytical plate-theory solutions. Windowed Fourier filtering followed by reliability-sorted phase unwrapping was evaluated on 96 simulated 256 × 256 interferograms. Under moderate decorrelation, 99.9% of pixels were correctly unwrapped at 10 fringes, with a filtered wrapped-phase RMSE of 0.30 rad; success decreased to 76.9% at 15 fringes and 15.0% at 25 fringes. Under strong decorrelation, the operating limit shifted to approximately 5–10 fringes. Detector SNR from 15 to 35 dB produced no meaningful performance trend because multiplicative decorrelation dominated. These findings indicate that the classical pipeline behaves as a threshold system governed primarily by fringe density and decorrelation. Experimental validation of the noise model remains necessary.

ACCEPTED

05.10.26

Keywords: *digital holographic interferometry; forward model; synthetic dataset; speckle decorrelation; phase unwrapping; windowed Fourier filtering; optical metrology.*



1. Introduction

A digital holographic interferometer records the wave scattered by an object on a sensor and reconstructs the complex field numerically. Subtracting the reconstructed phases of two object states gives a non-contact, full-field displacement map whose sensitivity is finer than one wavelength (Schnars & Jüptner, 2002), (Kreis, 2005). Phase-shifting acquisition (Yamaguchi & Zhang, 1997) is the usual way to retrieve the object field without spatial filtering.

Two effects limit how accurate the resulting phase map can be. The first is speckle decorrelation. The speckle pattern produced by a rough surface changes between the two states, so the phase noise is multiplicative and cannot be treated as purely additive (Goodman, 2020). The second is the 2π ambiguity:

the measured phase is known only modulo 2π and must therefore be unwrapped, and classical unwrapping algorithms spread errors once the noise is strong or the fringes are dense (Ghiglia & Pritt, 1998).

Neural networks have been proposed for speckle denoising (Montresor et al., 2020; Fang et al., 2022), phase unwrapping (Wang et al., 2022) and fringe analysis (Feng et al., 2019). All of them are trained on pairs consisting of a corrupted and a clean phase map. In an experiment, a clean map requires an additional independent measurement, which makes simulated data the practical alternative. Simulated data are useful only if they reproduce what makes real phase maps hard to process, above all the way decorrelation grows with fringe density. A simulation that simply adds Gaussian noise to an ideal phase does not do this.

The aim of this study is to provide a simulator of this kind and to put it to use. We (i) formulate a forward model of the DHI phase chain and implement a generator of wrapped phase maps whose ground truth is an analytical displacement field, and (ii) apply the generator to measure how a classical filtering-plus-unwrapping chain responds to changes in fringe density, detector SNR and decorrelation strength, which shows the regimes where a learned method has room to improve. The study complements our work on a joint denoising and unwrapping network (Akbarova & Toshpulatova, n.d.), which is outside its scope. All results refer to simulated data; no experimental holograms were recorded.

2. Materials and Methods

2.1. Phase–displacement relation

Consider a single illumination and observation geometry with laser wavelength λ and an angle α between the sensitivity vector and the surface normal. The interferometric phase is then related to the out-of-plane displacement d(x,y) by

$$\frac{4\pi}{\lambda} \cdot d_{x,y} \cdot \cos\alpha \qquad (1)$$

The measured quantity is the wrapped phase $\Delta\varphi_w = W[\Delta\varphi]$, where the operator W folds values into the interval $(-\pi, \pi]$. The simulations used λ = 532 nm, α = 0 and images of 256 × 256 pixels. The fringe count N_f is the total phase range divided by 2π: $N_f = [\max \Delta\varphi - \min \Delta\varphi]/2\pi$.

2.2. Displacement fields

The true displacements were taken from closed-form solutions of classical plate theory (Timoshenko & Woinowsky-Krieger, 1959) rather than from finite-element models. Three cases were used: (i) a clamped circular plate under uniform pressure, $w \propto (1 - r^2/a^2)^2$; (ii) a vibration mode of a simply supported rectangular plate, $w \propto \sin(m\pi x/a)\cdot\sin(n\pi y/b)$ with $m, n \in \{1, 2\}$; (iii) a simply supported square plate under uniform load, described by the Navier series $w \propto \Sigma \sin(m\pi x/a)\cdot\sin(n\pi y/a)/[mn(m^2 + n^2)^2]$ over odd m, n up to 11. The amplitude of each field was scaled so that the phase of Eq. (1) contained the required fringe count Nf, chosen between 2 and 25.

2.3. Speckle and noise model

Two independent, fully developed speckle fields, s_1 (state 1) and s_1', were generated as circular complex Gaussian random fields, smoothed with a Gaussian of 1.5 px and normalized to unit mean intensity. The field in state 2 is constructed as

$$s_2 = \rho \cdot s_1 \cdot \exp(i\Delta\varphi) + \sqrt{(1 - \rho^2)} \cdot s_1' \qquad (2)$$

$$\rho(x,y) = \rho_0 \cdot \exp[-(|\nabla\Delta\varphi|/g_c)^2] \qquad (3)$$

Equation (3) is a modelling assumption: the correlation ρ between the two speckle fields decreases as the local phase gradient, that is, the fringe density, increases. We set $\rho_0 = 0.95$ and used two values of g_c: 1.0 rad/px for moderate decorrelation and 0.6 rad/px for strong decorrelation. Neither value was fitted to experimental data. Additive detector noise n_1, n_2 (circular complex Gaussian, variance $10^{-SNR/10}$ for unit mean intensity) was then added to both fields, and the wrapped phase is

$$\Delta\varphi_w = arg[(s_2 + n_2)(s_1 + n_1)\dagger] \qquad (4)$$

ISSN: 2181-3337 | SCIENTISTS.UZ

The generator parameters are summarized in Table 1.

Parameter	Value	Comment
Image size	256 × 256 px	—
Wavelength, sensitivity angle	532 nm, α = 0	Eq. (1)
Displacement fields	3 analytical plate solutions	Section 2.2
Fringe count N_f	2, 5, 10, 15, 20, 25	Phase range / 2π
Speckle size	1.5 px (Gaussian smoothing)	Unit mean intensity
Decorrelation ρ_0; g_c	0.95; 1.0 (moderate) or 0.6 rad/px (strong)	Assumed, Eq. (3)
Detector SNR	15, 20, 25, 30, 35 dB	Additive, both fields

Table 1. Parameters of the synthetic data generator.

2.4. Classical processing chain

The reference method is a two-dimensional windowed Fourier filter (Kemao, 2007) followed by phase unwrapping. The wrapped phase is converted to exp(iΔφw) and analysed with a Gaussian window of σw = 6 px on a 13 × 13 grid of spatial frequencies (±0.9 rad/px, step 0.15 rad/px). Coefficients whose magnitude falls below 2.5 times a noise level, estimated as the median coefficient magnitude, are set to zero, and the field is then reconstructed. Unwrapping uses the reliability-sorted, non-continuous-path algorithm of Herráez et al. (Herráez et al., 2002) in its scikit-image implementation (van der Walt et al., 2014). The filter settings were identical for all conditions and were not tuned for any of them. For comparison, the noisy phase was also unwrapped directly, without filtering.

2.5. Metrics and experimental design

Three quantities were evaluated against the ground truth: (i) the wrapped-phase RMSE, which characterizes the filtering stage; (ii) the unwrapping success, defined as the fraction of pixels where the estimated phase deviates from the truth by less than π after a global multiple of 2π has been removed; and (iii) the computation time of the chain on one CPU core.

$$RMSE = \frac{\sqrt{\Sigma W[\Delta\varphi w - \Delta\varphi]^2}}{N} \quad (5)$$

Every condition was simulated 6 times (two realizations per displacement field, each with its own random seed), and results are reported as mean ± standard deviation over these 6 realizations. Two series were run: over N_f at 20 dB for both decorrelation regimes, and over SNR at N_f = 10 for moderate decorrelation. In addition, phase noise on a flat field (Δφ = 0) was measured for ρ_0 = 1.0, 0.9 and 0.8. The classical chain processed 96 interferograms in total (the point at N_f = 10 and 20 dB belongs to both series).

2.6. Check of the filter frequency range

The fixed frequency range of the filter (±0.9 rad/px) is narrower than the maximum local phase gradient at 15 or more fringes (about 1.1–2.0 rad/px). To test whether this limitation explains the failures, 3 realizations per condition were processed again at 15, 20 and 25 fringes (moderate decorrelation), with the range widened to 1.2 times the maximum gradient.

3. Results

3.1. Characteristics of the generator

Examples of generated data are shown in Fig. 1. With detector noise alone (ρ_0 = 1), the standard deviation of the flat-field phase noise dropped from 0.43 rad at 15 dB to 0.059 rad at 35 dB, roughly in proportion to $10^{-SNR/20}$ (Fig. 2). For ρ_0 = 0.9 it decreased only from 0.76 to 0.69 rad over the same range, and for ρ_0 = 0.8 from 0.96 to 0.92 rad; above about 25 dB the curves were flat. At N_f = 10, 30 dB and strong decorrelation, the standard deviation of the wrapped-phase error grew with the local phase gradient, from 0.53 rad where $|\nabla \Delta\varphi| < 0.1$ rad/px (mean ρ = 0.95) to 1.55 rad where $|\nabla \Delta\varphi| \geq 0.45$ rad/px (mean ρ = 0.30).

ISSN: 2181-3337 | SCIENTISTS.UZ

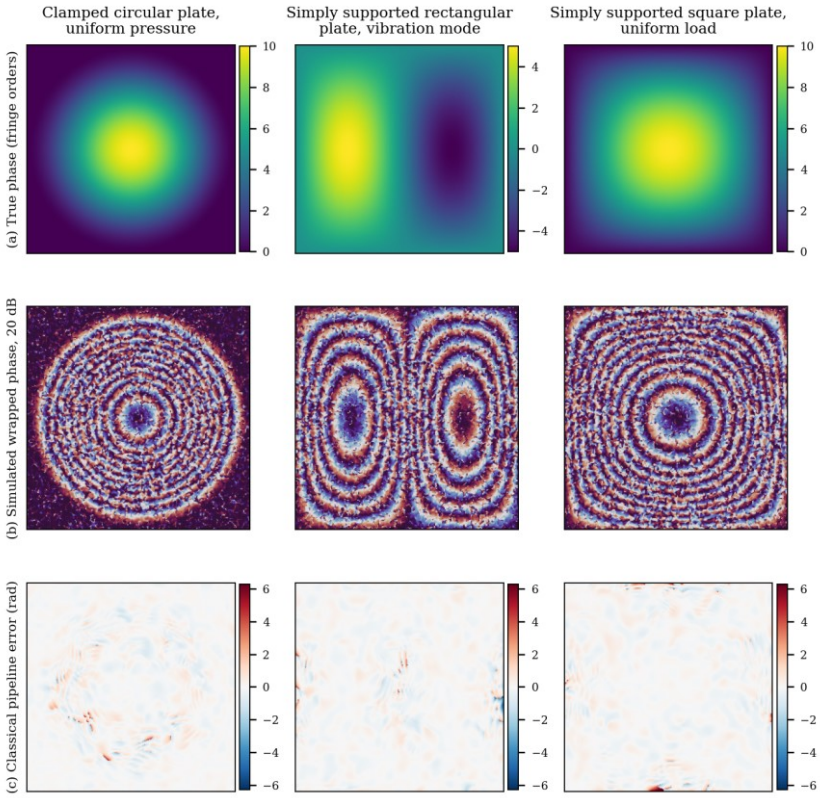


Figure 1. Generator output at N_f = 10, 20 dB and moderate decorrelation: (a) true phase in fringe orders; (b) simulated wrapped phase; (c) error of the WFF + unwrapping chain after removal of a global 2π multiple (clipped to ±2π).

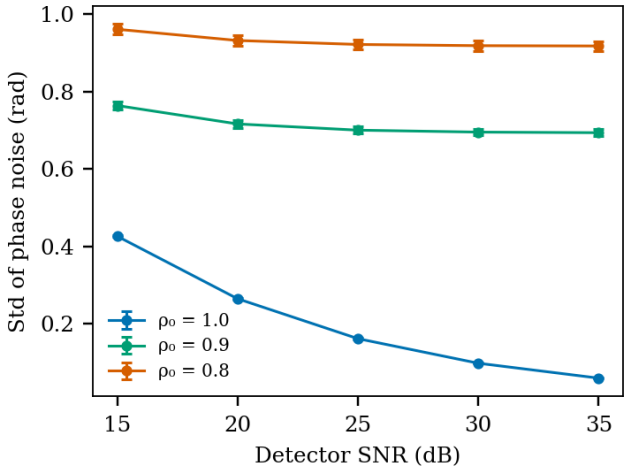


Figure 2. Standard deviation of the flat-field phase noise versus detector SNR for three values of ρ_0 (6 realizations; error bars show the SD).

3.2. Classical chain versus fringe count

Results of the fringe-density series at 20 dB are given in Table 2 and Fig. 3. Under moderate decorrelation, 99.9% of pixels were unwrapped correctly at 10 fringes, and the wrapped-phase RMSE after filtering was 0.30 rad (0.12 rad at 2 fringes). At 15 fringes the success dropped to 77% and the RMSE of the unwrapped phase rose to about 10 rad owing to 2π errors; at 20 and 25 fringes only 22% and 15% of pixels were correct. Under strong decorrelation the chain was reliable up to 5 fringes, gave 76% at 10 fringes and 8% at 15 fringes. Unwrapping without prior filtering succeeded for 98% of pixels at 5 fringes but for only 60% at 10 fringes (moderate decorrelation). Between 20 and 25 fringes the wrapped-phase RMSE after filtering (1.4–1.5 rad) was close to that of the noisy input (1.5 rad).

ISSN: 2181-3337 | SCIENTISTS.UZ

N_f	Moderate: correct pixels, %	Moderate: RMSE after WFF, rad	Strong: correct pixels, %	Strong: RMSE after WFF, rad	Unwrap only (moderate), %
2	100.0 ± 0.0	0.12 ± 0.00	100.0 ± 0.0	0.13 ± 0.01	99.4 ± 0.0
5	100.0 ± 0.0	0.16 ± 0.01	100.0 ± 0.0	0.25 ± 0.01	98.2 ± 0.4
10	99.9 ± 0.1	0.30 ± 0.02	76.4 ± 9.6	0.92 ± 0.02	59.6 ± 13.1
15	76.9 ± 9.3	0.89 ± 0.02	8.3 ± 2.9	1.47 ± 0.10	19.2 ± 14.1
20	22.1 ± 19.0	1.39 ± 0.08	6.3 ± 2.3	1.61 ± 0.12	9.7 ± 6.5
25	15.0 ± 23.3	1.47 ± 0.18	4.1 ± 0.7	1.64 ± 0.12	6.2 ± 3.3

Table 2. Classical chain versus fringe count at 20 dB (mean ± SD, 6 realizations per row). "Correct pixels" is the unwrapping success defined in Section 2.5.

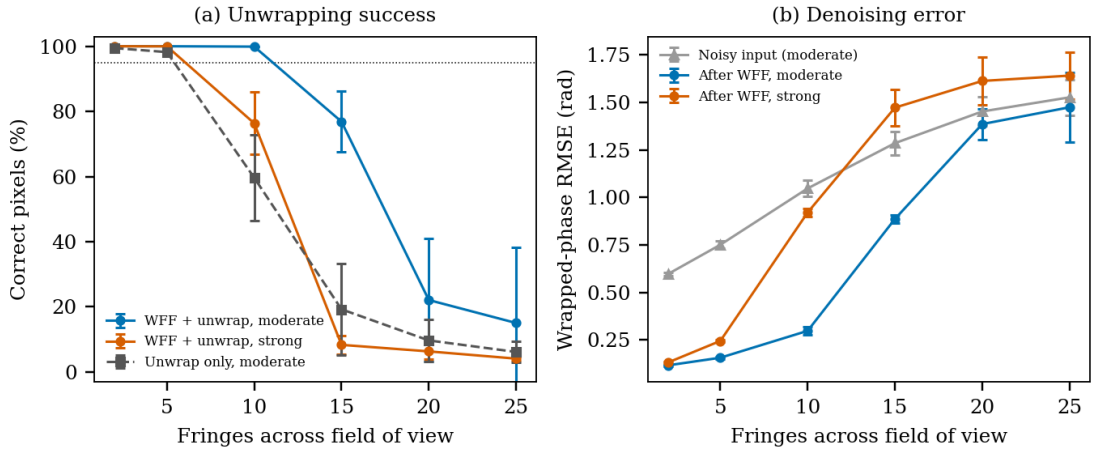


Figure 3. (a) Unwrapping success and (b) wrapped-phase RMSE versus fringe count at 20 dB. The dotted line in (a) marks 95%.

3.3. Classical chain versus detector SNR

The SNR series at 10 fringes and moderate decorrelation is presented in Table 3. Between 15 and 35 dB the success remained at 99.8–99.9% and the RMSE after filtering at 0.28–0.30 rad, with no visible trend. The mean computation time of the chain was 2.76 ± 0.09 s per 256 × 256 field, of which unwrapping accounted for 0.021 s.

SNR, dB	Correct pixels, %	RMSE after WFF, rad	RMSE of noisy input, rad
15	99.9 ± 0.0	0.28 ± 0.02	1.02 ± 0.06
20	99.9 ± 0.1	0.30 ± 0.02	1.05 ± 0.04
25	99.8 ± 0.1	0.29 ± 0.03	1.01 ± 0.06
30	99.8 ± 0.1	0.29 ± 0.02	1.03 ± 0.04
35	99.9 ± 0.1	0.30 ± 0.02	1.01 ± 0.06

Table 3. Classical chain versus detector SNR at N_f = 10, moderate decorrelation (mean ± SD, 6 realizations).

3.4. Effect of widening the filter frequency range

Extending the range to 1.2 times the maximum gradient (Section 2.6) did not improve the wrapped-phase RMSE after filtering, which was 0.95 rad at 15 fringes, 1.3–1.4 rad at 20 fringes and 1.4–1.6 rad at 25 fringes. The unwrapping success was 59–71% at 15 fringes and 3–10% at 20–25 fringes.

4. Discussion

The main finding is that the classical chain has a fairly sharp operating limit. Under moderate decorrelation it works well up to about 10 fringes and breaks down between 10 and 15; under strong decorrelation the breakdown moves to 5–10 fringes. The chain behaved as a threshold system: it was either

accurate or failing, with little in between. For this reason the mean RMSE of the unwrapped phase is a poor summary, and the success fraction should be reported alongside it. Pre-filtering with WFF extended the usable range from about 5 to about 10 fringes, but beyond 20 fringes it no longer improved the phase, since the RMSE after filtering was close to that of the noisy input.

The results point to decorrelation, not the filter, as the cause of the failures. Widening the filter band did not help (Section 3.4), so in this model the breakdown at high fringe density comes from phase information lost through decorrelation rather than from a limited filter range. The same conclusion follows from the flat-field and SNR series (Fig. 2, Table 3): above about 25 dB the phase error is set by decorrelation and no longer by the detector. The growth of the phase error with the local gradient (Section 3.1) is exactly the coupling between noise and fringe density that the model was built to reproduce.

These findings have two consequences for the design of training data. First, a learned method can show an advantage only near and beyond the classical limit, so a training set should contain fringe densities and decorrelation strengths on both sides of that limit. Second, a dataset that varies only the SNR would cover the wrong axis; the decorrelation parameters should be sampled explicitly.

The values obtained here, about 0.3 rad of wrapped-phase RMSE at 10 fringes and a fall in success between 10 and 15 fringes, are of the same order as the classical-chain figures assumed in our companion work (Akbarova & Toshpulatova, n.d.). They nevertheless apply to one specific model and to one untuned implementation of the filter and the unwrapper, and they should not be taken as the best that classical methods can achieve. The timing result likewise belongs to an unoptimized single-core implementation; it shows only that the filtering stage, not the unwrapping, dominates the cost of the classical chain.

Limitations. (1) All data are simulated; the agreement of Eqs. (2)–(3) with speckle decorrelation in a real interferometer has not been tested, and ρ_0 and g_c are assumed values. The next step is a comparison with experimental phase maps, for example the benchmark database of Montresor et al. (Montresor et al., 2020), using the distributions of local phase deviation and the residual-noise correlation length at matched fringe density. (2) The displacement fields are analytical plate-theory solutions; finite-element fields for more complex specimens and loading are not yet included. (3) Only out-of-plane displacement in a single-illumination geometry is modelled. (4) Each condition was simulated 6 times, so the standard deviations in Tables 2 and 3 are rough estimates. (5) Timing was measured on one CPU core with unoptimized code.

5. Conclusion

We developed a forward model of the DHI phase chain that combines multiplicative, fringe-density-dependent speckle decorrelation with additive detector noise, together with a generator of synthetic phase maps with analytical ground truth. Using it, a windowed Fourier filter followed by reliability-sorted unwrapping correctly unwrapped 99.9% of pixels at 10 fringes and 77% at 15 fringes under moderate decorrelation, and its operating range shrank to 5–10 fringes under strong decorrelation. Between 15 and 35 dB the result did not depend on the detector SNR. Before synthetic data from this model are used to train or qualify a measurement method, the model must be checked against experimental holograms.

REFERENCES

1. Akbarova, N. A., & Toshpulatova, D. (n.d.). Deep-learning-assisted digital holographic interferometry for non-contact measurement of deformation, vibration, and elastic properties [Manuscript submitted for publication].
2. Fang, Q., Xia, H., Song, Q., Zhang, M., Guo, R., Montresor, S., & Picart, P. (2022). Speckle denoising based on deep learning via a conditional generative adversarial network in digital holographic interferometry. *Optics Express, 30*(12), 20666–20683.
3. Feng, S., Chen, Q., Gu, G., Tao, T., Zhang, L., Hu, Y., Yin, W., & Zuo, C. (2019). Fringe pattern analysis using deep learning. *Advanced Photonics, 1*(2), 025001.

ISSN: 2181-3337 | SCIENTISTS.UZ

4. Ghiglia, D. C., & Pritt, M. D. (1998). *Two-dimensional phase unwrapping: Theory, algorithms, and software*. Wiley.
5. Goodman, J. W. (2020). *Speckle phenomena in optics: Theory and applications* (2nd ed.). SPIE Press.
6. Herráez, M. A., Burton, D. R., Lalor, M. J., & Gdeisat, M. A. (2002). Fast two-dimensional phase-unwrapping algorithm based on sorting by reliability following a noncontinuous path. *Applied Optics, 41*(35), 7437–7444.
7. Kemao, Q. (2007). Two-dimensional windowed Fourier transform for fringe pattern analysis: Principles, applications and implementations. *Optics and Lasers in Engineering, 45*(2), 304–317.
8. Kreis, T. (2005). *Handbook of holographic interferometry: Optical and digital methods*. Wiley-VCH.
9. Montresor, S., Tahon, M., Laurent, A., & Picart, P. (2020). Computational de-noising based on deep learning for phase data in digital holographic interferometry. *APL Photonics, 5*(3), 030802.
10. Schnars, U., & Jüptner, W. (2002). Digital recording and numerical reconstruction of holograms. *Measurement Science and Technology, 13*(9), R85–R101.
11. Timoshenko, S., & Woinowsky-Krieger, S. (1959). *Theory of plates and shells* (2nd ed.). McGraw-Hill.
12. van der Walt, S., Schönberger, J. L., Nunez-Iglesias, J., Boulogne, F., Warner, J. D., Yager, N., Gouillart, E., & Yu, T. (2014). scikit-image: Image processing in Python. *PeerJ, 2*, e453.
13. Wang, K., Kemao, Q., Di, J., & Zhao, J. (2022). Deep learning spatial phase unwrapping: A comparative review. *Advanced Photonics Nexus, 1*(1), 014001.
14. Yamaguchi, I., & Zhang, T. (1997). Phase-shifting digital holography. *Optics Letters, 22*(16), 1268–1270.